Available online at www.sciencedirect.com
SCIENCE DIRECT
Journal of Power Sources 155 (2006) 145–151
JOURNAL OF POWER SOURCES
www.elsevier.com/locate/jpowsour

Effect of cathode current-collecting layer on unit-cell performance of anode-supported solid oxide fuel cells

H.Y. Jung, W.-S. Kim, S.-H. Choi, H.-C. Kim, J. Kim, H.-W. Lee, J.-H. Lee *

Nano-Materials Research Center, Korea Institute of Science and Technology, 39-1 Hawolgok-dong, Seongbuk-gu, Seoul 136-791, Republic of Korea

Received 3 February 2005; accepted 9 May 2005
Available online 22 July 2005

Abstract

According to the characterization of the microstructure and properties of solid oxide fuel cells (SOFC) electrodes, it is essential to verify various processing variables to control microstructural parameters, such as particle size, composition and spatial distribution of the constituent phases of the electrode in order to reduce the ohmic and diffusional polarization losses of the unit-cell performance. From this viewpoint, a current-collecting layer with controlled microstructure very effectively enhances the unit-cell performance by reducing the ohmic and polarization resistance of the cathode. The maximum power density of a 5 cm × 5 cm unit-cell with the controlled current-collecting layer is ~1.5 W cm^{-2} at 750 °C, while a unit-cell without the layer is much lower, viz., 0.9 W cm^{-2}.

Keywords: Electrode; Current-collecting layer; Polarization loss; Cell performance; Solid oxide fuel cell; Power density

1. Introduction

The solid oxide fuel cell (SOFC) is expected to be a strong candidate for next generation power systems, due to its high efficiency, high waste-heat utilization, and low emission of pollutants to the environment [1]. At present, most research and development activities on SOFCs are directed to the development of a commercially viable technology with high electrochemical performance and long-term stability. To this end, many researchers have attempted to develop an intermediate- or low-temperature SOFC that can be operated between 600 and 750 °C [1,2].

To date, many investigations have focused on dynamic correlation of the electrodic functions of SOFC electrodes with their microstructure and corresponding electrochemical performance [3–10]. Based on the results of these investigations, most researchers contend that proper control of the microstructural parameters of the electrodes, such as particle size, porosity and spatial distributions of the constituent phases, is essential to reduce the ohmic and diffusional polarization losses of the unit-cells [3–10]. For example, in the case of an anode reaction under high load conditions, the reactant diffusion into the reaction site, which is normally located near the anode|electrolyte interface, is the overall rate-controlling step. Consequently, the structural features of the anode, e.g. pore size, volume fraction of the pores and tortuosity, become the main determining factors in controlling the diffusion rates of the reactant gases and the corresponding anode reaction [4]. On the other hand, in the cathode reaction, several groups have reported results that indicate the importance of the contribution of three-phase boundaries (TPB) within the electrode to the overall cathodic electrochemical reactions [5–7]. In particular, Tsai and Barnett [5] pointed out the detailed microstructural effects of the cathode, such as powder composition, size distribution, volume fraction, and phase distribution on the cathode performance. Moreover, Barbucci et al. [6] proposed a viable method to optimize the structure and composition of composite cathodes of SOFCs via experimental and modelling studies. In particular, they analyzed the influence of gas-phase diffusion in the interstices of the electrode structure and showed that

* Corresponding author. Tel.: +82 29585532; fax: +82 29585529.
E-mail address: jongho@kist.re.kr (J.-H. Lee).

0378-7753/$ – see front matter © 2005 Elsevier B.V. All rights reserved.
doi:10.1016/j.jpowsour.2005.05.015

the diffusion limitations became significant if the electrode was composed of the random packing of very small particles (particle diameter < 0.2 μm) [6,7].

It is also known that La(Sr)CoO_3 (LSCo) exhibits superior cathodic performance to LSM, e.g. the polarization of a LSCo cathode sputtered on YSZ is very small even at 800 °C [8]. On the other hand, LSCo tends to react more readily with YSZ electrolyte than LSM at high temperatures (≥1000 °C), and the resulting $La_2Zr_2O_7$ or $SrZrO_3$ compounds exhibit very high ohmic resistance [8]. Nonetheless, to our knowledge, there have been few reports on practical and convenient methods to prepare LSCo cathodes on a YSZ electrolyte without forming any by-products. Currently, the only available method is to use an interlayer on the YSZ electrolyte to prevent unfavourable solid-state reactions between the LSCo cathode and the YSZ electrolyte.

In relation to this unwanted reaction problem, we report here the fabrication conditions of LSCo-based SOFCs without any interfacial reaction and investigate the electrochemical performance of cells via various analysis techniques such as dc *I–V* electronic load and current interruption techniques. In addition, a study is made of the effect of cathode structure on the performance of anode-supported 5 cm × 5 cm unit-cells, particularly with regard to the efficiency of the current-collecting capability of the cathode on the power-generating characteristics of the unit-cells at intermediate temperatures of 600–800 °C.

2. Experimental

2.1. Fabrication of unit-cells

Fine yttria-stabilized zirconia (Tosoh, Japan), coarse yttria-stabilized zirconia (Unitec, USA), and nickel oxide (J.T. Baker, USA) powders were used to prepare the NiO–YSZ anode substrate. The granules of NiO–YSZ composite powders were compacted by uni-axially pressing into the green anode substrate. An anode functional layer, which had the same composition as the anode substrate but did not contain the coarse YSZ powder, was printed on the NiO–YSZ substrate via screen-printing. A YSZ electrolyte layer was also screen-printed on the anode functional layer and co-fired at 1400 °C in air for 3 h.

The cathode powders $(La_{0.7}Sr_{0.3})_{0.95}MnO_3$ (LSM) and $(La_{0.7}Sr_{0.3})_{0.95}CoO_3$ (LSCo) were synthesized via a modified glycine-nitrate-process. In order to prevent any interfacial reaction between the LSCo current-collector and YSZ electrolyte, a bi-layered cathode consisting of LSM–YSZ (60:40 wt.%) and LSM was applied. The cathode was then screen-printed on the sintered anode|electrolyte substrate. Two types of unit-cells were fabricated, namely, one with only the aforementioned bi-layered cathode and another with an additional LSCo current-collecting layer. All of the cathode layers were co-fired at 1150 °C in air for 3 h. The process yielded 5 cm × 5 cm unit-cells with l mm thickness. The electrochemical performance of these two types of unit-cells was determined in order to determine the effect of the current-collecting layer on the overall cathode performance.

2.2. Characterization of electrode microstructure

The electrical conductivity of the electrodes was measured by means of the dc four-point probe technique as a function of temperature. The porosity and pore distribution of electrodes were determined with mercury porosimetry and the gas permeability of the electrode was inspected with a perm-porometer (PMI, USA). The thermal expansion coefficient (TEC) of the electrode was measured with a dilatometer (NETZSCH, Germany). The electrode microstructure of the unit-cells was observed by means of scanning electron microscopy (Hitachi S-4200) and quantitatively analyzed by using commercial image analysis software (Image-Pro, USA) based on quantitative stereological theory.

2.3. Electrochemical characterization of cell performance

A ceramic–glass composite sealant and an Inconnel based interconnect were used for evaluating unit-cell performance. The flow channels of the interconnect were designed to have co-flow of fuel and oxidant gas. The current–voltage and current–power characteristics were measured with a SOFC test station (Toyo, SAT890-100 W) in the temperature range of 600–800 °C. Air was used as an oxidant and moisturized hydrogen with 3% water (H_2 + 3% H_2O) was used as a fuel. For electrochemical characterization, a current-interruption technique was used to measure the ohmic loss (IR-drop) of the cells.

3. Results and discussion

3.1. Microstructure and its related physical properties of the electrodes

According to our previous investigations [9–11] on the electrode microstructure and its related physical properties, proper manipulation of the processing variables for the electrode fabrication is very important with respect to obtaining the best unit-cell performance. In particular, the electrical and/or electrochemical properties of the electrode, which determine the ohmic and diffusional polarization loss in unit-cells, are normally tailored not only by appropriate connection of the electrical conducting path but also by that of the gas-diffusion path. Thus, in this study, we have controlled the microstructure of each electrode in order to obtain better electrical conductivity and gas permeability.

Scanning electron micrographs of unit-cells with and without the current-collecting layer are given in Fig. 1. As shown in the cross-sectional view, each unit-cell consists

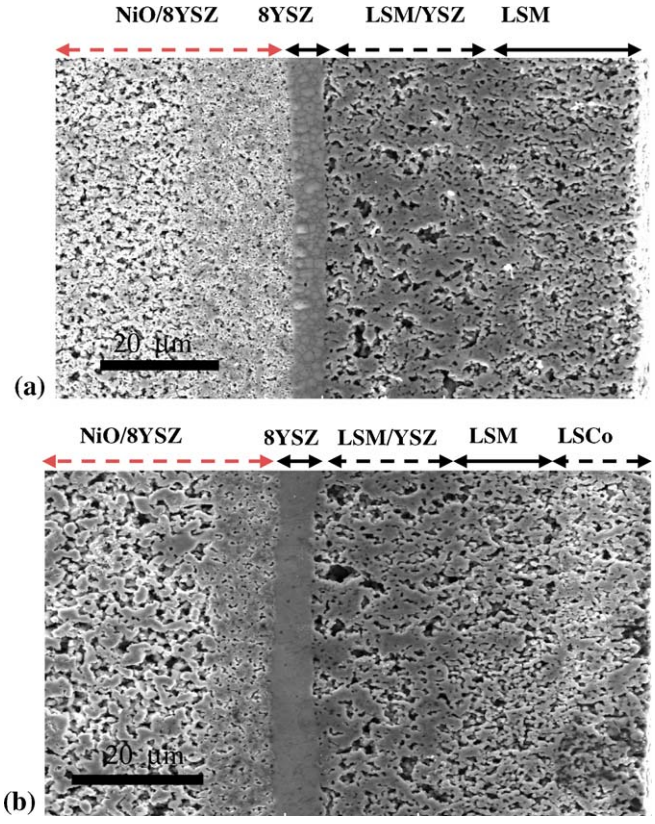

Fig. 1. Cross-sectional view of unit-cells: (a) without LSCo layer; (b) with LSCo layer.

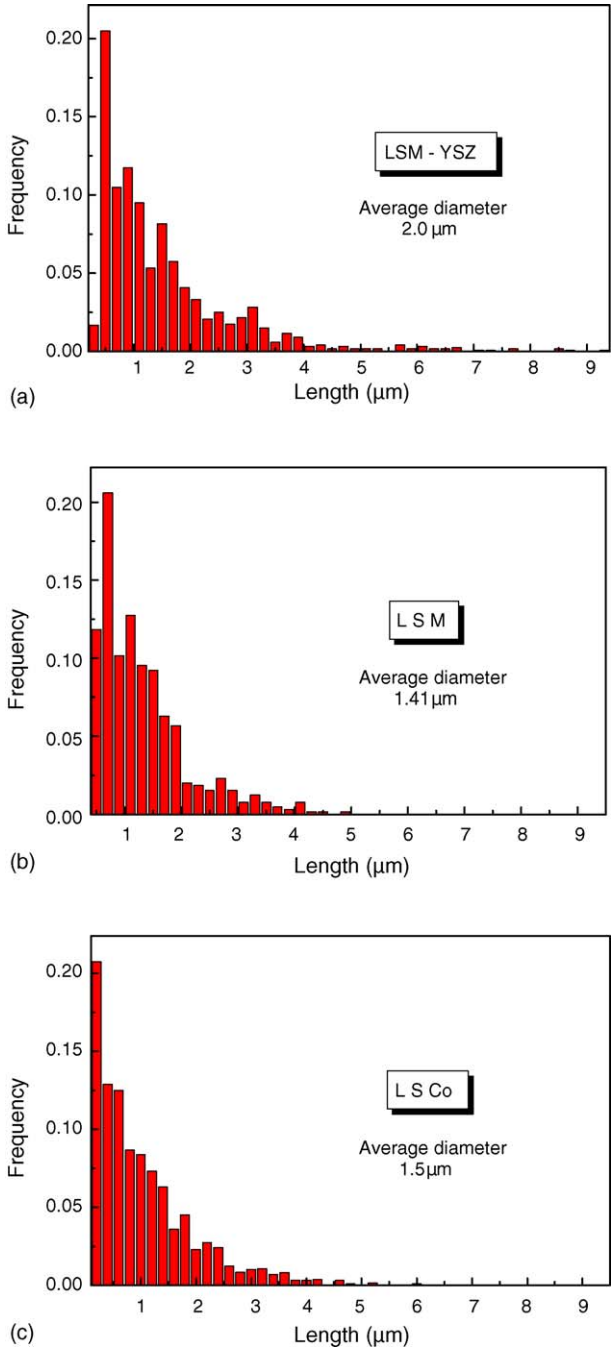

Fig. 2. Pore-size distribution of multi-layered cathode: (a) LSM–YSZ composite layer; (b) LSM layer; (c) LSCo layer. Obtained by quantitative image analysis of BSE image of unit-cells.

of five or six different layers that include a single functional layer for the cathode and anode side correspondingly. There is not a large difference in the thicknesses of the anode (∼1.0 mm) and anode functional (15–20 μm) and electrolyte layers (6–8 μm) in both types of unit-cells. The main difference lies in the constitution of the cathode layers, even though the overall cathode thickness was similar at around 50 μm.

Only the YSZ electrolyte layer is dense, having a sintered density of over 97%, whereas the anode and cathode layers are relatively porous, see Fig. 1. The electrolyte layer contains no connected pores or pinholes, which results in almost no gas permeability (Darcy's constant < 0.0001).

By contrast, the anode consists of two layers, i.e. the anode substrate and the anode functional layer. The porosity of these layers is quite different. According to the microstructural analysis via our recently developed quantitative image analyzing technique [12], the Ni–YSZ anode substrate has a porosity of over 40% and the average pore size is around 1.4 μm, while the anode functional layer had a porosity of 10% and 0.3 μm pore size.

The pore-size distribution of the multi-layered cathode is shown in Fig. 2. The porosity of the cathode is around 36–40% and the average pore diameter is 1.4–2 μm. The corresponding values for the current-collecting layer are about 32 and 1.15 μm, respectively. The pore-size distribution of the LSM–YSZ layer was very broad up to ∼9 μm diameter while the LSCo layer showed much smaller pore size and a narrow distribution.

The electrical conductivity of the LSM–YSZ composite and LSM cathode is ∼93 and ∼150 S cm^{-1}, respectively, while that of LSCo is much higher at around 1100 S cm^{-1} at 800 °C. With respect to general practice in SOFC development [2], these values fulfil the necessary conditions of cathode conductivity. The thermal expansion coefficients (TEC) of the LSM–YSZ composite and LSM bulk sam-

Table 1
Typical physical properties of SOFC unit-cell components

Components	Properties					
	TEC[a] ($\times 10^{-6}$, K^{-1})	Porosity (%)	Average pore diameter (μm)	Gas permeability[a] (Darcy's)	Conductivity at 800 °C[a] ($S\,cm^{-1}$)	Thickness
Anode						
Substrate	14.0	42	1.40	0.034	1011	1.0 mm
Functional	14.0	9.7	0.33	–	–	15–20 μm
Electrolyte[a]	10.5	<3	–	<0.0001	0.047	~6–8 μm
Cathode						
LSM–YSZ	11.5	40	2.00	0.054	93	~25 μm
LSM	13.0	36	1.40	0.037	152	~13 μm
LSCo	17–20	32	1.15	0.030	1100	~12 μm

[a] Results were obtained from bulk samples, TEC was measured in the range 200–900 °C.

ple are $11.5 \pm 0.3 \times 10^{-6}$ and $13.0 \pm 0.2 \times 10^{-6}$ cm cm^{-1} K, respectively, which are relatively comparable with those of the anode and electrolyte. On the other hand, the average TEC of LSCo is much higher at about 18.8×10^{-6} cm cm^{-1} K, which could cause a TEC mismatch problem between the unit-cell components. Nonetheless, neither cracking nor delamination occurs during the fabrication and operation of the unit-cells. The image analysis results and other microstructure related physical properties of each cell component are summarized in Table 1.

3.2. Power-generating characteristics of unit-cells

The cell performance curves of the 5 cm × 5 cm anode supported cells with or without a LSCo layer are given in Fig. 3. The operating conditions were 3% H_2O added hydrogen as a fuel and air as an oxidant. The fuel utilization condition of 60% for each unit-cell was determined from the criterion of ~0.7 V at 800 °C and the air flow was fixed as twice the stoichiometric amount ('2 stoichs'). As shown in Fig. 3, the open-circuit voltages of both types of cell is not significantly different (it falls in the range of 1.15–1.20 V), whereas the power-generating characteristics are extremely different. The maximum power density of 1.5 W cm^{-2} is achieved in the unit-cell with the LSCo layer at 750 °C, while a power density of 0.95 W cm^{-2} is obtained in the unit-cell without the LSCo layer. Considering that there is no difference in the composition and microstructure of the anode and electrolyte layers, the different power-generating characteristics of the two types of unit-cell are mainly attributed to the existence of the cathode current-collecting layer, which may change the contact resistance of the cathode with the metallic interconnector.

A typical example of separation of the power losses of the unit-cell without a LSCo layer at 700 °C is given in Fig. 4. The voltage losses during cell operation are normally divided into: (i) ohmic loss, due to the ohmic resistance (R_s) of the unit-cell components; (ii) polarization resistance (R_p) due to each electrodic reaction. Furthermore, the ohmic resistance (R_s) of the unit-cell which is normally known to have a very strong dependence on features of the cell geometry, such as the thickness of each cell component and the contact geometry between the current-collector and the electrodes and between the electrodes and electrolyte [13], can be divided into the electrolyte resistance (R_{elyt}), the electrode material

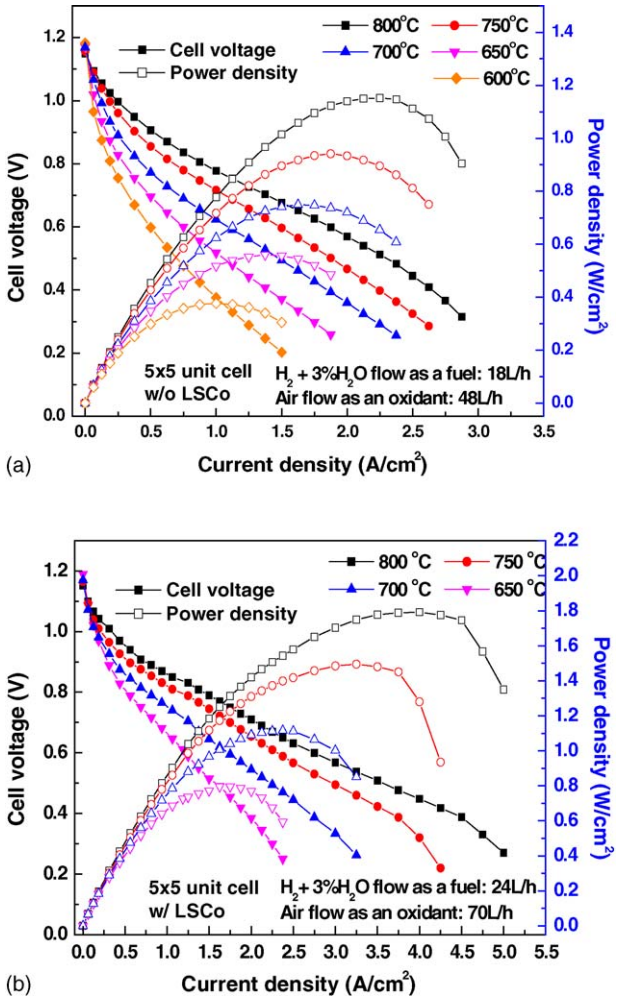

Fig. 3. Power-generating characteristics of unit-cells with effective area of 16 cm^2 under various operating temperatures: (a) without LSCo layer; (b) with LSCo layer. Gas flow conditions of fuel and air were: (a) 18 and 48 L h^{-1}; (b) 24 and 70 L h^{-1}.

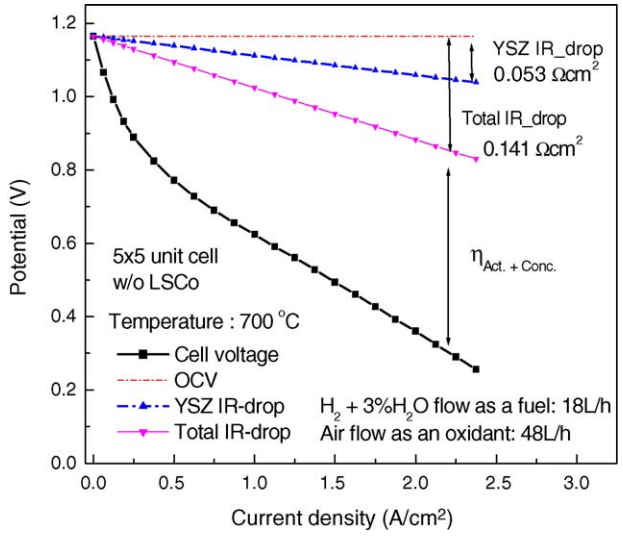

Fig. 4. Separated cell performance losses from total IR drop measured by current interruption technique (5 cm × 5 cm unit-cell without LSCo layer at 700 °C).

resistance (R_{eltrod}), and the contact resistance due to non-optimized contact and current collection ($R_{contact}$).

To break down the ohmic contribution of each unit-cell component to the whole power loss of the cell, a dc current interruption technique was employed. Estimated values of the ohmic loss factors were obtained in the form of area specific resistance (ASR, R_s), which can be a unique value of the cell regardless of the current density for all experimental condition. The estimated values are summarized in Table 2.

In Table 2, we also present the YSZ ASR (R_{elyt}), calculated from the bulk conductivity of the YSZ electrolyte, in order to estimate the ratio of the electrolyte resistance to the total ohmic ASR of the unit-cells. Both the total ohmic resistance and the electrolyte resistance increase as the temperature is decreased, while the ratio of the electrolyte resistance to the total resistance is different in the two types of cell. For the cell with a LSCo layer, the electrolyte resistance occupies the major portion of the total resistance, and thus the remaining ohmic resistance ($R_s - R_{elyt}$) is much lower than that estimated for the cell without a LSCo layer. These results are attributed to the LSCo layer lowering the ohmic resistance of the cells, particularly the contact resistance between the cathode and the metallic interconnector.

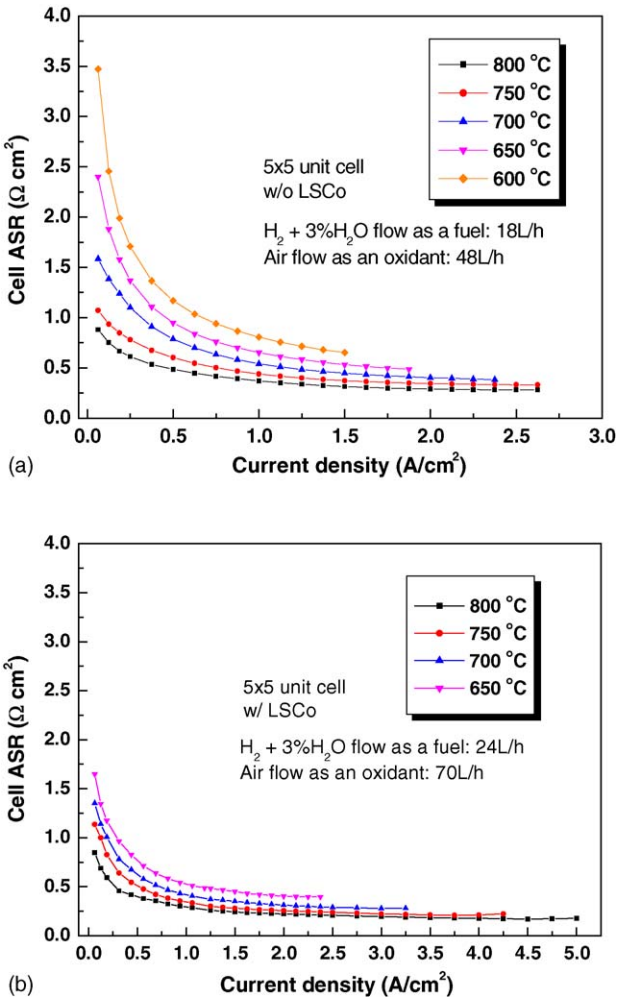

Fig. 5. Measured area specific cell resistances of unit-cell: (a) without LSCo layer; (b) with LSCo layer at various operating temperatures.

The overall cell performance obtained from the *I–V* characteristics for both types of unit-cell at various operation temperatures is presented in Fig. 5. The cell performance is estimated in terms of the area specific resistance of the cell (cell ASR) rather than the power density, which has been more frequently employed as a characteristic value to represent overall cell performance. Such an interpretation of cell performance with cell ASR is known to be much less dependent on the individual test conditions compared with power

Table 2
Total ohmic ASR (R_s) measured via current interruption method and YSZ–ASR (R_{elyt}) calculated by conductivity of YSZ bulk

Temperature (°C)	YSZ bulk conductivity ($\times 10^{-2}$ S cm^{-1})	R_{elyt}[a] (Ω cm^2)	R_s (Ω cm^2)		Contribution R_{elyt}/R_s (%)		$R_{contact}$ (Ω cm^2)	
			Without LSCo	With LSCo	Without LSCo	With LSCo	Without LSCo	With LSCo
600	0.41	0.195	0.285	–	68.4	–	0.090	–
650	0.79	0.101	0.202	0.150	50.0	67.3	0.101	0.049
700	1.5	0.053	0.141	0.108	37.6	49.1	0.088	0.055
750	2.7	0.030	0.106	0.069	28.3	43.5	0.076	0.039
800	4.7	0.017	0.070	0.045	24.3	37.8	0.053	0.028

[a] YSZ electrolyte thickness, 8 μm.

Table 3
Ohmic ASR measured via current interruption method and cell ASR estimated from dc *I–V* characteristics

Temperature (°C)	Ohmic ASR (R_s, $\Omega\,cm^2$)		Cell ASR at 1.0 A cm^{-2} ($\Omega\,cm^2$)		Polarization ASR (R_p) at 1.0 A cm^{-2} ($\Omega\,cm^2$)	
	Without LSCo	With LSCo	Without LSCo	With LSCo	Without LSCo	With LSCo
600	0.285	–	0.806	–	0.521	–
650	0.202	0.150	0.652	0.525	0.450	0.375
700	0.141	0.108	0.541	0.417	0.400	0.309
750	0.106	0.069	0.439	0.344	0.333	0.275
800	0.070	0.045	0.371	0.293	0.301	0.248
E_A (eV)	0.56	0.68	0.31	0.33	0.23	0.23

density, and thus is more suitable to compare objectively each unit-cell performance [14].

As shown in Fig. 5, the cell ASR is, in fact, not a constant value and varies with respect to the current density in contrast to the ohmic ASR in Table 2. Therefore, it is generally necessary to introduce specific criteria to determine the characteristic ASR of each unit-cell. In general, the characteristic ASR of the unit-cell is determined at the point where the ASR changes rather slowly with respect to the variation of current density. Hence, in most cases, ASR is calculated at the current level where the corresponding voltage is at an interval of 0.5–0.7 V [14]. In the present case, the ASR value is assigned at a current density of 1.0 A cm^{-2} as the characteristic ASR of the corresponding unit-cell.

The cell ASRs decrease rapidly at low current density whereas those at higher current density decrease relatively slowly with a flat-linear shaped curve. Further, the cell ASR of the unit-cell containing the LSCo layer has a, relatively lower value than that of the unit-cell without a LSCo layer for all experimental conditions. This indicates that the unit-cell containing the LSCo layer is superior in cell performance to that without the LSCo layer. Values of the cell ASR at a constant current density (1.0 A cm^{-2}) as well as to the measured total ohmic ASR from the current interruption experiment are summarized in Table 3.

According to the comparison in Table 3, it is evident that the improved cell ASRs of the LSCo cell originate not only from the improved ohmic resistance but also from the improved polarization resistance. This indicates that adoption of the LSCo current-collecting layer can enhance the overall cathodic reactions. The apparent thermal activation energy E_A can also be calculated from the temperature dependence of the ASRs given in Table 3. According to the analysis, the activation energy of the ohmic resistance of the unit-cell containing the LSCo layer is higher than that of the cell without the LSCo layer. This suggests that the electrolyte resistance of the unit-cell with a LSCo layer gives a greater contribution to the overall ohmic resistance than in the cell without a LSCo layer.

From these results, it is concluded that the proper use of a current-collecting layer makes a strong contribution to the enhancement of the unit-cell performance by reducing not only the ohmic resistance but also the electrode polarization resistance. Nevertheless, further electrochemical characterization of the detailed polarization phenomena in unit-cell operation should be undertaken in order to verify the manner and degree to which the current-collecting layer influences the individual polarization losses of the electrodic reaction. This will be the topic of a forthcoming paper.

4. Conclusions

Anode-supported 5 cm × 5 cm unit-cells with an optimized electrode microstructure have been fabricated. In particular, a novel current-collecting layer has been adopted to assess the efficiency of the current-collecting capability of the cathode on the unit-cell performance. According to the analysis, a current-collecting layer with controlled microstructure is very successful in terms of enhancing the unit-cell performance by reducing the ohmic and polarization resistance of cathode. The maximum power density of a unit-cell with the current-collecting layer is approximately 1.8 W cm^{-2} while that of a unit-cell without the layer is less than 1.2 W cm^{-2} at 800 °C. This demonstrates the positive effect of the current-collecting layer on unit-cell performance.

Acknowledgements

This work has been supported by the Core Technology Development Program for Fuel Cell and the NRL Program of the Ministry of Science and Technology of Korea and the Korea Institute of Science and Technology Evaluation and Planning.

References

[1] N.Q. Minn, J. Am. Ceram. Soc. 76 (1993) 563.
[2] N.Q. Minh, T. Takahashi, Science and Technology of Ceramic Fuel Cells, Elsevier, Amsterdam, 1995 (Chapter 1–5).
[3] S.P. Jiang, J. Power Sources 124 (2003) 390.
[4] H. Yakabe, M. Hishinuma, M. Uratani, Y. Matsuzaki, I. Yasuda, J. Power Sources 86 (2000) 423.
[5] T. Tsai, S.A. Barnett, Solid-State Ionics 93 (1997) 207.
[6] A. Barbucci, R. Bozo, G. Cerisola, P. Costamagna, Electrochim. Acta 47 (2002) 2183.

[7] P. Holtappels, C. Bagger, J. Eur. Ceram. Soc. 22 (2002) 41.
[8] O. Yamamoto, Y. Takeda, R. Kanno, M. Noda, Solid-State Ionics 22 (1987) 241.
[9] J.-H. Lee, H. Moon, H.-W. Lee, J. Kim, J.-D. Kim, K.-H. Yoon, Solid-State Ionics 148 (2002) 15.
[10] J.-H. Lee, J.-W. Heo, D.-S. Lee, J. Kim, G.-H. Kim, H.-W. Lee, H.-S. Song, J.-H. Moon, Solid-State Ionics 158 (2003) 225.
[11] D.-S. Lee, J.-H. Lee, J. Kim, H.-W. Lee, H.-S. Song, Solid-State Ionics 166 (2004) 13.
[12] K.-R. Lee, S.H. Choi, J. Kim, H.-W. Lee, J.-H. Lee, J. Power Sources 140 (2005) 226.
[13] J. Fleig, J. Maier, J. Electrochem. Soc. 44 (1997) 302.
[14] M. Mogensen, P.V. Hendriksen, in: S.C. Singhal, K. Kendall (Eds.), High Temperature Solid Oxide Fuel Cells, Elsevier, UK, 2003, p. 272.